REVISION 2 – after Proofs

The IR vibrational properties of six members of the garnet family: a quantum mechanical ab initio study

ROBERTO DOVESI[1,*], MARCO DE LA PIERRE[1], ANNA M. FERRARI[1], FABIEN PASCALE[2], LORENZO MASCHIO[1] AND CLAUDIO M. ZICOVICH-WILSON[3]

[1]*Dipartimento di Chimica IFM, Università di Torino and NIS -Nanostructured Interfaces and Surfaces - Centre of Excellence, http://www.nis.unito.it, Via P. Giuria 7, 10125 Torino, Italy*

[2]*5Q, rue du Beaujolais, 54500 Vandœuvre-lès-Nancy, France*

[3]*Facultad de Ciencias, Universidad Autónoma del Estado de Morelos, Av. Universidad, 1001, Col. Chamilpa, 62209 Cuernavaca (Morelos), Mexico*

ABSTRACT

The IR vibrational properties and the corresponding reflectance spectra of the six most common members of the garnet family (pyrope $Mg_3Al_2Si_3O_{12}$, almandine $Fe_3Al_2Si_3O_{12}$, spessartine $Mn_3Al_2Si_3O_{12}$, grossular $Ca_3Al_2Si_3O_{12}$, uvarovite $Ca_3Cr_2Si_3O_{12}$ and andradite $Ca_3Fe_2Si_3O_{12}$) were simulated at the ab initio level with the CRYSTAL09 code by using a large all-electron Gaussian-type basis set and the B3LYP hybrid functional. The 17 IR active F_{1u} transverse optical (TO) and longitudinal optical (LO) frequencies, the oscillator strengths, the high frequency and static dielectric constants and the reflectance spectrum were computed. The agreement with experiments for the TO and LO peaks is always excellent, the mean absolute difference for the whole set of data (overall 178 peaks) being 5 cm^{-1}. Oscillator strengths, calculated from the mass-weighted effective Born charges, are found in semi-quantitative agreement with the experimental data. The reflectance spectra, simulated through the classical dispersion relation, turn out to reproduce extremely well the experimental curves. The availability of the full set of simulated frequencies and intensities, obtained by using uniform computational tools (computer code, variational basis sets, density functional) permits to establish correlations between IR wavenumbers and structural features, suggested but only partially documented in the past.

KEYWORDS garnets, IR frequencies, IR intensities, reflectance spectrum, ab-initio calculations, all-electron gaussian basis sets, B3LYP functional, CRYSTAL code

[*] E-mail: *roberto.dovesi@unito.it*

INTRODUCTION

Garnets $X_3^{II}Y_2^{III}Si_3O_{12}$ are important rock-forming silicates, as major constituents of the Earth's upper mantle and relevant phases of high-pressure metamorphic rocks in the Earth's crust (Deer et al. 1992). From the technological point of view, they are largely used for a variety of industrial applications, for example filtration media and abrasives, thanks to their recyclability and high hardness (Olson 2001). Pyrope $Mg_3Al_2Si_3O_{12}$ (Prp), almandine $Fe_3Al_2Si_3O_{12}$ (Alm), spessartine $Mn_3Al_2Si_3O_{12}$ (Sps), grossular $Ca_3Al_2Si_3O_{12}$ (Grs), uvarovite $Ca_3Cr_2Si_3O_{12}$ (Uv) and andradite $Ca_3Fe_2Si_3O_{12}$ (Adr) are the most abundant members of the family.

Garnets, despite their relatively complex structure, represent excellent reference systems for the study of the vibrational properties of silicates. Their large unit cell (80 atoms) is characterized by high symmetry (the space group is $Ia\bar{3}d$). Building blocks are SiO_4 tetrahedra sharing corners with YO_6 octahedra; X^{2+} cations are in dodecahedral coordination. Because of the high symmetry, garnets present a relatively simple vibrational spectrum (17 IR and 25 Raman active modes). The vibrational properties have been extensively investigated with various experimental techniques (Hofmeister and Chopelas 1991a; Hofmeister et al. 1996; McAloon and Hofmeister 1995; Kolesov and Geiger 1998, 2000; Chopelas 2005). In particular, a detailed infrared (IR) reflectance study on single crystal samples of five end-members of the garnet family was carried out by Hofmeister (Hofmeister and Chopelas 1991a; Hofmeister et al. 1996; McAloon and Hofmeister 1995). This nearly complete and homogeneous set of data represents an ideal reference for a computational investigation.

In previous papers (Pascale et al. 2005a, 2005b; Zicovich-Wilson et al. 2008; Valenzano et al. 2009; Ferrari et al. 2009; Valenzano et al. 2010; Dovesi et al. 2009b), Transverse Optical (TO) and Longitudinal Optical (LO) IR-active frequencies, together with TO-LO splitting values, were calculated and compared with experimental data for each of the six garnets. The agreement between simulated and observed values was found to be excellent, as indicated by the mean absolute

difference $\overline{|\Delta|}$ (smaller than 10 cm^{-1}).

Recently new tools have been implemented in the CRYSTAL code, that permit to evaluate the oscillator strengths (Maschio et al. 2011) and the dielectric tensor (Ferrero et al. 2008a, 2008b). The comparison with experiments can then be extended to these two new features, and to the reflectance spectrum R(ν), that is now generated automatically by the CRYSTAL code (preliminary results have been published for Alm by Ferrari et al. 2009). As R(ν) is the experimental primary information, from which position and intensity of the peaks are obtained, the accessibility of $R^{calc}(\nu)$ permits a more direct comparison with experiments.

The presentation and discussion of these new features represents the main motivation for the present paper. A second non minor motivation is the following: the availability of the full set of data for the six compounds permits to establish correlations between spectral features, chemical composition and structural data that in the past have been suggested in many papers, but only partially documented, due to incompleteness of data and accuracy problems.

In the present work a comprehensive analysis of the IR vibrational properties of the six garnets is presented, that includes: classification of the modes, TO and LO wavenumbers, TO-LO splitting, oscillator strengths and reflectance spectra. The equilibrium geometry and the high frequency and static dielectric constants have also been obtained. The present study represents the most systematic and extended comparison of computed and experimental data for the vibrational properties of crystalline solids, as it involves 178 wavenumbers, 82 oscillator strengths, 5 reflectance spectra.

COMPUTATIONAL METHOD

Calculations have been performed by using an all-electron Gaussian-type basis set, the hybrid B3LYP functional (Becke 1993; Koch and Holthausen 2000) and the CRYSTAL09 code (Dovesi et al. 2009a). The B3LYP functional was shown to reproduce the vibrational frequencies of ionic and

semi-ionic compounds, such as silicates, in excellent agreement with experimental data (Zicovich-Wilson et al. 2004; Prencipe et al. 2004; Pascale et al. 2005a, 2005b; Orlando et al. 2006; Zicovich-Wilson et al. 2008; Valenzano et al. 2009; Ferrari et al. 2009; Valenzano et al. 2010; Dovesi et al. 2009b)).

Oxygen, silicon, aluminum, calcium and magnesium have been described by (8s)-(411sp)-(1d), (8s)-(6311sp)-(1d), (8s)-(611sp)-(1d), (8s)-(6511sp)-(21d) and (8s)-(511sp)-(1d) contractions, respectively. For transition metal ions a (8s)-(64111sp)-(411d) type basis has been used, as described in previous works (Pascale et al. 2005a, 2005b; Zicovich-Wilson et al. 2008; Valenzano et al. 2009; Ferrari et al. 2009; Valenzano et al. 2010). For spessartine, andradite and uvarovite an f shell has been added. This modification and others, performed on Al (split of a sp contraction) and Ca (split of a d contraction) in order to check the stability of the results, turned out to have a very limited influence on wavenumbers and intensities. The exponent of the most diffuse sp and d shell has been reoptimized for each compound. The complete basis sets and details on the computational parameters can be found on the CRYSTAL Web site (http://www.crystal.unito.it/supplement/index.html), where input and output files related to the calculations are reported.

The level of accuracy in evaluating the Coulomb and Hartree-Fock exchange series is controlled by five parameters (Dovesi et al. 2009a) that have been set to 7 7 7 8 16. In the case of almandine, they have been increased to 8 8 8 8 18, to improve numerical accuracy as a way to cure the slow SCF convergence, due to the Jahn-Teller nature of the ground state, that is related to the d^6 electronic configuration of the Fe^{2+} cation. The threshold on the self-consistent field (SCF) energy has been set to 10^{-8} Hartree for the optimizations, and to 10^{-10} Hartree for the construction of the Hessian.

The reciprocal space has been sampled according to a regular sublattice with shrinking factor (Dovesi et al. 2009a) IS=3, corresponding to four independent **k** vectors in the irreducible part of the Brillouin zone. The exchange-correlation contribution to the Fock matrix has been evaluated by

numerical integration over the unit cell volume. Radial and angular points of the grid are generated through Gauss-Legendre radial quadrature and Lebedev two-dimensional angular points distributions. In the present work, a (75,974) grid has been used, which corresponds to a pruned grid with 75 radial and 974 angular points (XLGRID keyword in the CRYSTAL09 manual, Dovesi et al. 2009a). Details about the grid generation, the number of points in reciprocal space, and their influence on the accuracy and cost of calculation can be found in Pascale et al. 2005a; Zicovich-Wilson et al. 2008.

As regards the compounds containing transition metal ions, it is well known that the high-spin solution is more stable than the low-spin one at ambient conditions; extremely high pressures are required to induce the transition to a low-spin state (Badro et al. 2004; Tsuchiya et al. 2006; Rouquette et al. 2008). In order to drive the convergence of our computational scheme towards the high spin electronic configuration, an initial guess has been given for the density matrix, defining the spin state (either α or β) of each transition metal ion and the amount of n_α - n_β electrons per unit cell.

Structures have been optimized by using the analytical energy gradients with respect to atomic coordinates and unit cell parameters (Doll et al. 2001; Doll 2001; Civalleri et al. 2001), within a quasi-Newton scheme combined with the BFGS algorithm for Hessian updating (Broyden 1970; Fletcher 1970; Goldfarb 1970; Shanno 1970). Convergence has been checked on both gradient components and nuclear displacements, for which the default values (Dovesi et al. 2009a) have been chosen.

The calculation of the TO vibrational frequencies at the Γ point has been performed within the harmonic approximation; the mass-weighted Hessian matrix W is constructed by numerical differentiation of the analytical gradients with respect to the atomic cartesian coordinates. The calculated (optimized) equilibrium geometry is taken as reference. Details on the calculation of vibrational frequencies can be found in Pascale et al. 2004; Zicovich-Wilson et al. 2004; Born and

Huang 1954, Sections 5, 10, 34, 35.

The oscillator strength f_j of the j^{th} IR-TO normal mode of an isotropic crystal has been computed by means of the mass-weighted effective mode Born charge $\bar{Z}_j^2$, evaluated through well localized Wannier functions (Zicovich-Wilson et al. 2001, 2002; Noel et al. 2002), according to the expression

$$f_j=\frac{4\pi}{\Omega}\frac{\bar{Z}_j^2}{\nu_j^2}, \qquad [1]$$

where ν_j is the corresponding TO frequency and Ω is the cell volume.

The effect of anharmonicity for this class of compounds has been estimated to be quite small for frequencies (not larger than 2÷3 cm^{-1}). We are unable to estimate the effect on oscillator strengths, however.

The reflectance spectrum $R(\nu)$ for normal incidence is defined as (Decius and Hexter 1977)

$$R(\nu)=\left|\frac{\sqrt{\varepsilon(\nu)}-1}{\sqrt{\varepsilon(\nu)}+1}\right|^2. \qquad [2]$$

According to the classical dispersion relation (Decius and Hexter 1977; Born and Huang 1954; Gonze and Lee 1997; Kleinmann and Spitzer 1962), the complex dielectric function $\varepsilon(\nu)$ of an isotropic crystal is defined as

$$\varepsilon(\nu)=\varepsilon_\infty+\sum_j\frac{f_j\nu_j^2}{\nu_j^2-\nu^2-i\nu\gamma_j}, \qquad [3]$$

where ν_j, f_j and γ_j are the TO peak position, the oscillator strength and the damping factor, respectively, and ε_∞ is the high frequency dielectric constant. As the harmonic model is used in our simulation, we are unable to compute the γ_j damping factors; their values have been guessed as discussed in the "Infrared reflectance spectra" Section.

The electronic high frequency contribution ε_∞ has been calculated through the Coupled-Perturbed KS/HF (Kohn-Sham/Hartree-Fock) scheme (Ferrero et al. 2007, 2008a, 2008b, 2008c; 2009); this

quantity is almost constant with respect to frequency in the IR range, as electronic transition energies are very large compared to IR transition energies.

According to Equation 3, the static dielectric constant ε_0 is equal to

$$\varepsilon_0=\varepsilon_\infty+F=\varepsilon_\infty+\sum_j f_j, \qquad [4]$$

where the ionic contribution F is evaluated as the sum of the oscillator strengths.

Calculated and experimental wavenumbers ν_i and oscillator strengths f_i have been compared through four global indices defined as (x_i is either ν_i or f_i)

$$\overline{|\Delta|}=M^{-1}\sum_{i=1}^{M}\left|x_i^{calc}-x_i^{exp}\right|; \qquad [5]$$

$$\overline{\Delta}=M^{-1}\sum_{i=1}^{M}\left(x_i^{calc}-x_i^{exp}\right); \qquad [6]$$

$$\left|\Delta_{max}\right|=max\left|x_i^{calc}-x_i^{exp}\right|, \qquad i=1,2,....M; \qquad [7]$$

$$\overline{|\Delta|}^{*}=M^{-1}\sum_{i=1}^{M}\left|x_i^{calc}-x_i^{exp}-\overline{\Delta}\right|; \qquad [8]$$

where M is the number of data in the set, $\overline{|\Delta|}$ is the mean absolute difference between the calculated and the experimental values, $\overline{\Delta}$ is the mean difference, $\left|\Delta_{max}\right|$ is the maximum absolute difference, $\overline{|\Delta|}^{*}$ is the mean absolute difference computed after shifting the frequencies by the mean difference $\overline{\Delta}$.

Calculated and experimental reflectance spectra R(ν) have been compared by using the root mean square RMS, defined as

$$RMS=\sqrt{N^{-1}\sum_{i=1}^{N}\left\{\left[R(\nu_i)^{calc}\right]^2-\left[R(\nu_i)^{exp}\right]^2\right\}}, \qquad [9]$$

where N is the number of frequency values at which the reflectance curve has been computed.

Graphical animations of the normal modes are available on the CRYSTAL Web site

(http://www.crystal.unito.it/prtfreq/jmol.html), so that the reader can directly interpret the "nature" of the mode (stretching, bending, rotation of the tetrahedra, translation of the X^{2+} cation, etc) in a simple and intuitive manner.

RESULTS AND DISCUSSION

The garnet structure is highly symmetric: the space group is $Ia\bar{3}d$; the point group is O_h, with 48 symmetry operators. The X, Y and Si atoms are in dodecahedral (D_2), octahedral (S_6) and tetrahedral (S_4) special positions, respectively, whereas O atoms are in a general position.

Table 1 reports structural data for the six compounds, documenting the good agreement between calculated and experimental values. Cell parameters are overestimated by about 1%; similar differences are found for the X-O_1, Y-O and Si-O distances; in the case of X-O_2 the overestimation can reach 2%. These discrepancies are usual when the B3LYP functional is adopted.

The increase of the lattice parameter along the series correlates with the X and Y cation ionic radii (see Table 1), thus confirming experimental observations (Novak and Gibbs 1971).

The decomposition of the reducible representation built on the basis of the cartesian coordinates of the atoms in the unit cell leads to the following symmetry assignment of the 240 normal modes (this analysis is performed automatically by the CRYSTAL code):

$$\Gamma_{total} = 3A_{1g} \oplus 5A_{2g} \oplus 8E_g \oplus 14F_{1g} \oplus 14F_{2g} \oplus 5A_{1u} \oplus 5A_{2u} \oplus 10E_u \oplus 18F_{1u} \oplus 16F_{2u}.$$

55 modes are inactive, 25 are Raman active ($3A_{1g} \oplus 8E_g \oplus 14F_{2g}$) and 17 are IR active ($F_{1u}$ symmetry; one additional F_{1u} mode corresponds to translations).

Comparison between computed and experimental wavenumbers

Tables 2-7 report the complete set of computed infrared TO and LO wavenumbers, oscillator strengths and TO-LO splitting for the six compounds. From the experimental side (Hofmeister and Chopelas 1991a; Hofmeister et al. 1996; McAloon and Hofmeister 1995; Hofmeister, private communication), all the 17 TO and LO wavenumbers are available for Prp, Alm, Sps and Adr; in

the case of Grs, only 16 TO and LO distinct wavenumbers are available, since mode 4 was classified as a doublet (McAloon and Hofmeister 1995). Only five out of seventeen peaks are available for Uv, coming from a private communication by Hofmeister. For the TO modes, the agreement between experiment and theory is excellent, the mean absolute difference $\overline{|\Delta|}$ ranging from 3.4 cm^{-1} (Grs) to 7.3 cm^{-1} (Adr), with a mean value for the full set (89 modes overall), $\overline{|\Delta|}^{TO}_{total}$, equal to 5.2 cm^{-1}. The mean difference evaluated over the complete set of data $\overline{\Delta}^{TO}_{total}$ is only -2.0 cm^{-1}.

The largest difference $|\Delta_{max}|^{TO}_{total}$ is 23.3 cm^{-1}; only in two cases the absolute total difference $|\Delta\nu|$ exceeds 20 cm^{-1} (mode 2 of Alm and mode 14 of Prp), in one additional case it exceeds 15 cm^{-1} (mode 1 of Prp). Overall, only in nine additional cases $|\Delta\nu|$ is larger than 10 cm^{-1}: mode 7 of Prp, modes 1 and 2 of Sps and six frequencies of Adr (modes 6, 7, 8, 15, 16 and 17); in one case the computed wavenumber (mode 8 of Grs) cannot be assigned to an experimental counterpart, see Tables 2-7. The largest discrepancies between computed and observed values can be ascribed to difficulties in both the experimental procedures and in the computational setup.

On the experimental side (Hofmeister and Chopelas 1991a; Hofmeister et al. 1996; McAloon and Hofmeister 1995; Hofmeister, private communication), the primary outcome is the reflectance spectrum (see Equation 2). A Kramers-Kronig analysis is applied to $R(\nu)$ in order to derive the dielectric function $\varepsilon(\nu)$: the transverse optical frequencies $\nu_{TO,j}$ are defined by the maxima of the imaginary part of $\varepsilon(\nu)$ and the positions of the longitudinal optical modes $\nu_{LO,j}$ are derived from the minima of $Im(1/\varepsilon(\nu))$. The Kramers-Kronig analysis also provides a first estimate of the oscillator strengths f_j and the full widths at half heights γ_j of each mode. A classical dispersion analysis (Decius and Hexter 1977; Born and Huang 1954; Gonze and Lee 1997; Kleinmann and Spitzer 1962) is thus employed in order to construct a synthetic spectrum from a set of damped oscillators (the j^{th} normal mode being characterized by $\nu_{TO,j}$, f_j and γ_j), as expressed in Equation 3. The final

experimental values for f_j and γ_j are obtained by best fit of the experimental R(ν) spectrum through Equations 2 and 3. As a result of this rather complex procedure, several features of the spectrum (instrumental limitations, low intensity, background noise, overtones, peak superpositions) can affect the experimental estimate of the three sets of parameters, which show then a certain degree of uncertainty.

For instance, two of the modes with large $|\Delta\nu|$ are below 150 cm^{-1}, in a region of the spectrum that is characterized by low signal-to-noise ratio; in the case of Prp, two different wavenumbers (134.4 and 105 cm^{-1}) were suggested in two different experiments (Hofmeister and Chopelas 1991b; Hofmeister et al. 1996) for the lowest frequency mode, corresponding to the computed peak at 114.6 cm^{-1}. The other two modes that show large discrepancies with respect to the observed counterpart are the 673.3 cm^{-1} peak of Prp assigned to the experimental mode at 650 cm^{-1} ($|\Delta\nu|$ = 23.3 cm^{-1}) and the 404 cm^{-1} peak of Grs without any experimental counterpart; however both modes are characterized by a very low computed oscillator strength; the difficulty in detecting these peaks through the Kramers-Kronig analysis combined to the requirement of a complete set of 17 vibrations probably induced Hofmeister and coauthors (Hofmeister and Chopelas 1991a; Hofmeister et al. 1996; McAloon and Hofmeister 1995) to a questionable assignment: the 650 cm^{-1} peak (Prp) was in fact reported as very broad and weak (Hofmeister et al. 1996), and the mode at 241.4 cm^{-1} (Grs) was inferred to be a doublet (McAloon and Hofmeister 1995).

On the computational side, the adopted functional, despite its excellent behavior in describing the vibrational spectra of both molecules and solids, performs poorly in the low frequencies range (Maschio et al. 2011). Modes that can be interpreted as translations of the ”X” cations undergo a frequency downshift if the computed equilibrium lattice parameter is larger than the experimental one, as is the case when using B3LYP. Therefore discrepancies in this region can partly be attributed to the adopted functional.

In order to verify this issue, additional calculations were performed at the experimental cell volume (E.V., fractional coordinates being optimized anyhow) for all compounds but Alm (the SCF cycle

for Alm converges very slowly, as discussed in the "Compuational Method" Section, so that the CPU time required is quite large). Results are shown in Tables 8 and 9.

The full set of TO frequencies and oscillator strengths of Sps are reported in Table 8. Frequencies shifts $\Delta\nu_{calc,j}^{O.V.}$ vary from +4.4 to +23.1 cm^{-1}, with respect to the corresponding values computed at the optimized cell volume (O.V.); the mean difference $\overline{\Delta}_{calc}^{O.V.}$ is +12.1 cm^{-1}. This frequency upshift is due to a steeper electronic potential, which is in turn related to the decrease of the interatomic distances when using the experimental instead of the optimized lattice parameter. The mean absolute difference $\overline{|\Delta|}_{exp}$ with respect to the experimental data increases to 10.2 cm^{-1} (to be compared with 4.2 cm^{-1} in the case of the calculation at the optimized cell volume, Table 4). However, if all frequencies are shifted by the mean difference ($\nu_j^* = \nu_j - \overline{\Delta}_{exp}$), the mean absolute difference $\overline{|\Delta|}_{exp}^{*}$ (the star reminding the rigid shift) is only 5.1 cm^{-1}. Thus, the main effect of reducing the cell volume is a systematic, almost rigid, upwards shift (this rigid shift is obviously much larger in percentage for a frequency in the 100-200 cm^{-1} region than for higher frequencies). In summary, Table 8 shows that high frequencies are accurate at the optimized cell volume, whereas low frequencies are better reproduced by adopting the experimental volume. When looking at the other members of the family (see Table 9), all trends observed for Sps are confirmed.

We will see in the following that the effect of the volume change on the IR intensities is much more dramatic than the rigid shift observed for the frequencies.

As regards the LO modes, the statistical indices for the full set of frequencies $\overline{|\Delta|}_{total}^{LO}$, $|\Delta_{max}|_{total}^{LO}$ and $\overline{\Delta}_{total}^{LO}$ are 5.0, 28.2 and -2.1 cm^{-1}, respectively; these total values are similar to the TO ones. This similarity is not surprising, as only a small set of modes shift significantly in going from TO to LO. Among the 89 LO modes, nine $|\Delta\nu|$ exceed 10 cm^{-1}; of these, only three exceed 15 cm^{-1}. Two of them concern Prp and are associated to the TO modes that showed the same anomalous

behavior, see Tables 2-7. The third one is mode 9 in Grs; this is a low intensity mode, corresponding to the experimental wavenumber at 450 cm^{-1}, which was stated to be a weak shoulder (McAloon and Hofmeister 1995).

TO-LO splitting

In the experimental papers by Hofmeister and collaborators (Hofmeister and Chopelas 1991a; Hofmeister et al. 1996; McAloon and Hofmeister 1995), the problem of the one-to-one correspondence between TO and LO modes (TO-LO splitting or shift) is discussed at length. A pairing scheme is proposed, according to which LO wavenumbers are usually higher than the TO ones (the TO-LO shift is positive), in such a way that the corresponding TO and LO modes occupy the same position in the corresponding sets ordered by increasing wavenumber. In some cases, however, inversions appear: as the TO-LO shift is related to the strength of the oscillator, inversions are observed when a low intensity TO mode is just above (in the sequential order) and close (in the wavenumbers scale) to a TO mode with high intensity (Hofmeister and Chopelas 1991a; Hofmeister et al. 1996; McAloon and Hofmeister 1995). Inversions proposed by experimentalists are underlined in Tables 2-7.

The issue of the TO-LO pairing is however odd-defined, as confirmed by the fact that different experimental studies carried out by the same authors propose different inversions (Hofmeister and Chopelas 1991a; Hofmeister et al. 1996; McAloon and Hofmeister 1995). As discussed in our previous works (Zicovich-Wilson et al. 2008; Valenzano et al. 2009; Ferrari et al. 2009), the TO-LO one-to-one correspondence is possible without ambiguity only in the cases where a single mode exists for each Irreducible Representation of the group at the Γ point; in all other cases the two sets of modes (LO and TO) are independent, as resulting from independent diagonalizations of the W and $W + W^{NA}$ dynamical matrices, where W^{NA} is the non analytical correction (see Born and Huang 1954, Sections 5, 10, 34, 35; and Umari et al. 2001). In the limit of low polarization, one can however try to establish some link between LO and TO modes, under the

hypothesis that W^{NA} modifies only (or mainly) diagonal terms of W (Zicovich-Wilson et al. 2008). In order to establish such a link, we introduced the overlap criterion, based on the evaluation of the (non-symmetric) overlap matrix between TO and LO eigenvectors. The TO-LO correspondence is then based on the obvious observation that very similar modes feature eigenvectors that overlap to a large extent, whereas dissimilar modes do not. TO modes reported in Tables 2-7 are ordered by increasing frequency. The LO mode in a given line is the one with the maximum overlap with the TO mode in the same line. The overlap S is given in percent in the last column of the Tables. LO frequencies in bold character denote inversions in the increasing frequency sequence. The $\delta\nu$ column gives the TO-LO splitting evaluated on the basis of the overlap correspondence.

It turns out that:

- In most cases, the TO-LO overlap is larger than 75%; for these modes the TO-LO correspondence is clearly defined and turns out to be in agreement with experimentalists (Hofmeister and Chopelas 1991a; Hofmeister et al. 1996; McAloon and Hofmeister 1995). When the overlap is smaller, the correspondence is doubtful, as supported by the fact that in some cases our attributions differ from the experimentalists' ones (compare bold and underlined oscillator strengths in Tables).

  All the modes featuring large TO-LO splittings (see statements below) show overlaps equal to or smaller than 75% (down to 52%); the reason is that a large TO-LO shift is associated to large W^{NA} diagonal and off-diagonal contributions.

  Notably, in all the six garnets, the three modes with highest wavenumbers show low overlap values and present a high degree of mixing among them.

- The shift is larger than 50 cm^{-1} in 13 out of 102 modes; all these cases correspond to TO modes featuring the highest values of the product "$f_j \cdot \nu_j^2$" for each compound, as can be easily verified (bold oscillator strengths in Tables). The quantity "$f_j \cdot \nu_j^2$" is directly related to the IR intensity of vibrational modes: it is the numerator of the terms composing the dielectric function and corresponding to each damped oscillator (see also IR intensities A_j in Zicovich-

Wilson et al. 2008). Among the remaining modes, 74 show shifts smaller than 20 cm^{-1}.

- 23 wavenumber inversions are observed for the six garnets (bold LO wavenumbers in Tables). All these inversions take place immediately after vibrational modes featuring large TO-LO splittings and "$f_j \cdot \nu_j^2$" values (see statement above), with the only exception of mode 7 of Prp.

  Most of the inversions observed in the present work were proposed by experimentalists too (Hofmeister and Chopelas, 1991a; Hofmeister et al. 1996; McAloon and Hofmeister 1995) (underlined wavenumbers in Tables). Discrepancies occur in correspondence with modes featuring small TO-LO overlaps.

According to the present findings, it seems that the relevant features of the TO-LO assignment, namely large splittings, inversions and doubtful correspondences, are associated to high intensity IR modes (i.e. modes featuring high "$f_j \cdot \nu_j^2$" values).

Oscillator strengths

The oscillator strengths (f), given in Tables 2-7, show a qualitative agreement between simulation and experiment. The calculated peaks with high f always correspond to experimental peaks with high f; the absolute values are however in most of the cases quite different; for Alm, for example, the three most intense f are: f_j^{calc} = 2.77, 3.53 and 1.50 and f_j^{exp} = 0.9, 1.9 and 1.55 (modes 1, 2 and 10); for Adr, they are: f_j^{calc} = 3.54 and 1.19 and f_j^{exp} = 2.9 and 0.9 (modes 7 and 10). f^{calc} are in general higher than f^{exp}.

To deepen our analysis, let us compare the sums $F^{exp} = \sum_j f_j^{exp}$ and $F^{calc} = \sum_j f_j^{calc}$, that are given in Table 10. These quantities represent the ionic contribution to the static dielectric constant; F^{calc} is always larger than F^{exp}, by +36% (Prp), +32% (Alm), +30% (Sps), +26% (Grs), +6% (Adr) (experimental data not available for Uv). Independent experimental values $\Delta\varepsilon = \varepsilon_0 - \varepsilon_\infty$ (see Table 10) fall in between F^{exp} and F^{calc} in four out of five cases, slightly closer to F^{calc}. Both F^{calc} and F^{exp}

seem then to be affected by a certain error.

When passing from F to $\Delta F=\sum_j |\Delta f_j|$, that is the sum of the absolute differences between calculated and experimental f, the situation is still not satisfactory. ΔF is 3.61 (Prp, 31% of the corresponding F), 4.45 (Alm, 39%), 3.92 (Sps, 41%), 2.62 (Grs, 46%), 1.98 (Adr, 25%).

A careful inspection of Tables 2-7 shows that the discrepancies are mostly due to:

(i) low frequency modes (say below 200 cm^{-1});

(ii) modes characterized by very close frequencies (grouped f_j in Tables).

As regards point (i) two possible reasons for the large differences can be (i1) the overestimation of the lattice parameter by the B3LYP scheme (see Table 1); (i2) the lower accuracy of the experimental setup at the low wavenumbers (low signal-to-noise ratio).

In order to verify the former hypothesis (effect of the too long lattice parameters produced by B3LYP), it is worth comparing the oscillator strengths computed at the calculated optimized lattice parameter (O.V) with the ones obtained at the experimental lattice parameter (E.V., see also the "Comparison between computed and experimental wavenumbers" Section). The whole set of values is provided in the case of Sps in Table 8. The discrepancy with respect to experiment largely reduces; for example, $\overline{|\Delta f|}_{exp}$ and $|\Delta f_{max}|_{exp}$ go from 0.23 and 1.58 (optimized geometry) to 0.13 and 0.56 (experimental geometry), respectively. The sum of the oscillator strengths F reduces from 9.50 to 8.11, approaching the experimental Δε value (8.41, see Table 10). Thus, the overall quality of the computed oscillator strengths significantly improves. By looking at individual oscillator strengths, we notice that the by far largest deviations $\Delta f_{calc,j}^{O.V.}$ arise at low frequencies or for high intensity modes (e.g. modes 1,2 and 10). In these cases, $\Delta f_{calc,j}^{O.V.}$ values are negative and contribute to improve the overall agreement with experiment. These modes mainly involve X cation translations (see the "Correlation between vibrational modes and structure" Section): as the lattice parameter reduces, the X cations occupy sites of reduced sizes. As a consequence, their motion is more constrained,

and the corresponding polarization reduced.

All these trends are confirmed in the case of the other compounds (see Table 9). The improved agreement with experiment of mode 1 of Prp is particularly noticeable: f_j reduces from 5.13 to 2.37, which is only 0.47 larger than the experimental value (1.9). As Mg is the smallest X cation, and then can oscillate more than the other cations in the dodecahedral cage, the overestimation of the lattice parameter has an incredibly large effect on f_j. We can then conclude that the use of the experimental cell volume on the one side shifts by a nearly constant amount the frequencies, on the other side modifies in a very different way the calculated oscillator strengths, improving noticeably the ones of the low frequency modes (among the most intense) and the general agreement with experiment.

Concerning point (ii), we must notice that the one-to-one correspondence between calculated and experimental peaks, performed on the basis of the sequential order of the frequencies, might be wrong when peaks are very close. Moreover, when modes are close in frequency (and then the corresponding peaks overlap), the deconvolution of the experimental spectrum through a best fit process can be affected by large errors, due to the strong correlation between the parameters describing the intensity of these peaks. This is supported by the observation that the differences Δf_j for the couples of bracketed peaks (see Tables 2-7) are large, opposite in sign and nearly complementary; if the sum of the two f_j is considered, then Δf_j strongly reduces.

On the basis of these observations, the (ii) cases were included in the statistical indices after having summed up the intensities, whereas the (i) cases were simply excluded. This strategy largely reduces the sum of absolute differences $\Delta F'$, to 0.92 (Prp, 20% of the corresponding F' value), 0.80 (Alm, 18%), 0.94 (Sps, 21%), 1.30 (Grs, 27%) and 1.33 (Adr, 19%), thus supporting our interpretation of the origin of the discrepancies Δf_j (the prime sign reminds that these quantities are calculated with reference to the reduced set of f_j).

Infrared reflectance spectra

An important ingredient for the construction of the reflectance spectrum is the high frequency dielectric constant ε_∞, computed by means of a CPKS scheme (Ferrero et al. 2007, 2008a, 2008b, 2008c; 2009). Calculated values are 2.74 (Prp), 3.23 (Alm), 3.08 (Sps), 2.78 (Grs), 3.24 (Uv) and 3.40 (Adr). Differences with respect to experiment are always negative: -12%, -4%, -5%, -7%, -6% and -4%, respectively. With the exception of Prp, the results are thus quite satisfactory.

The reflectance spectra $R^{calc}(\nu)$ are computed from the dielectric function according to Equation 2. The latter is built starting from a set of damped oscillators (one for each normal mode) characterized by the oscillator frequencies ν_j (the IR-TO wavenumbers), the oscillator strengths f_j and the damping factors γ_j. The latter are not available from ab-initio calculations and must be guessed according to some criteria. Three sets of values were used in the present simulations: i) a constant mean value $\overline{\gamma} = 9$ cm^{-1} for the full set of data, corresponding to the average of the experimental values; ii) the set of experimental values γ_j^{exp}; iii) the set of fitted values γ_j^{fit} obtained from a best-fit procedure between $R^{calc}(\nu)$ and $R^{exp}(\nu)$.

These different choices were compared in the case of Grs. The set of experimental (Hofmeister and Chopelas 1991a) damping factors γ_j^{exp} (see Table 5) provides the dotted curve shown in Figure 1. The root mean square (RMS) among the experimental and calculated reflectance curves was calculated over the 551 points of the two datasets (explored interval 0-1100 cm^{-1}, with a step of 2 cm^{-1}) and taken as a figure of merit for the quality of our computed spectra; in this case it is equal to 0.081. The set of γ_j^{fit} (see Table 5) provides the dashed curve in Figure 1, that shows a striking agreement with $R^{exp}(\nu)$ (RMS=0.063). The residual mismatch is due either to small details of the experimental spectrum with no counterpart in the $R^{calc}(\nu)$ (e.g. the band around 500 cm^{-1}) or to the small discrepancies occurring between calculated and experimental ν_j and f_j (e.g. peaks around 850 cm^{-1}). Finally, the solid curve in Figure 1 was obtained by using $\overline{\gamma} = 9$ cm^{-1} for all modes. The RMS is equal to 0.099, not much worse than for γ_j^{exp} and γ_j^{fit} (less than a factor 2 larger). We

decided to use the constant value ($\bar{\gamma}$ = 9 cm^{-1}) for all the systems in order to reduce the semiempirical character of our R^{calc} (ν) (see also Maschio et al. 2011; De La Pierre et al. 2011). It should be noticed that the damping factor values influence only the amplitude of the peaks, not their positions.

Computed and experimental (except from Uv) reflectance spectra R(ν) related to the six garnets are shown in Figure 2. An example of the real and imaginary parts of ε(ν), that are used for computing R^{calc}(ν), is also given in Figure 3 for Adr. The agreement between computed and experimental curves is impressively good. In most of the cases a shift of the peaks along the wavenumber axis is observed in the low-frequency region, due to mismatches between computed and observed TO wavenumbers (see discussion in the "Comparison between computed and experimental wavenumbers" Section). Differences concerning the amplitudes of the peaks are mainly related to the use of the constant value $\bar{\gamma}$, as pointed out above. It turns out that the quality of the computed vibrational frequencies and oscillator strengths is sufficient for an excellent description of the reflectance spectra of crystalline systems, once a reasonable $\bar{\gamma}$ value is chosen. The quality of the results is constant along the family, the RMS being 0.106 (Prp), 0.115 (Alm), 0.118 (Sps), 0.099 (Grs), 0.128 (Adr).

Correlation between vibrational modes and structure

Isotopic mass substitution was used to evaluate the participation of the various atoms to the vibrational modes in the different regions of the spectrum, to interpret the nature of the modes (see also the graphical animations on the CRYSTAL Website – http://www.crystal.unito.it/prtfreq/jmol.html) and to identify trends, if any, along the garnet series. In the present study, the dynamical matrix W of the six systems was modified by: i) augmenting the mass of the X cation by 20%, or ii) reducing the mass of the Y cation by 20%; the resulting shifts in frequency are given in Tables 11 and 12 and in Figures 4 and 5.

Let us consider first the seven highest frequency modes (see Table 11). The three modes above 800 cm^{-1} (15-17) shift by less than 1 cm^{-1} upon isotopic substitution, and are then totally independent from X and Y. As regards the four other modes (11-14), with frequencies ranging from 429 (Adr) to 673 (Prp) cm^{-1}, they show some dependence on both cations (X and Y). In particular, modes 12 of Prp, Alm and Sps and 13 of Prp, Alm, Sps and Grs shift by more than 3%, reaching also 5.0% in the Prp case. This relatively small dependence on the cation mass confirms that these modes are mostly related to internal SiO_4 tetrahedra motions.

This hypothesis is supported by Figure 4, where the corresponding frequencies are plotted against the lattice parameter of each garnet. The dependence turns out to be nearly linear; taking as a reference the best-fit straight line for each mode, only one frequency deviates by an amount larger than 15 cm^{-1}. Such behaviour suggests that the main factor affecting the frequencies of these modes is the size of the unit cell: the larger the cell, the looser the potential (electronic and short range repulsion) perceived by the SiO_4 tetrahedra, the smaller the frequencies. The obtained trends are in good agreement with the ones reported in Hofmeister and Chopelas 1991a.

As expected, the effect of the isotopic substitution is more relevant for the ten lowest frequency modes. All these modes were classified in three classes, which are also highlighted in Table 12 and Figure 5: 1) Y dominated modes, when $\Delta_{up}/\Delta_{down} > 2$ and $\Delta_{up} > 3\%$ (overlined, light grey symbols); 2) X dominated modes, when $\Delta_{down}/\Delta_{up} > 2$ and $\Delta_{down} > 3\%$ (underlined, dark grey symbols); 3) "neutral" modes, when none of the previous conditions is satisfied (regular, black symbols). Δ_{up} (Δ_{down}) is the shift obtained by decreasing (increasing) the mass of Y (X) cation by 20%. The number of modes classified as "X dominated" and "Y dominated" according to the (somehow arbitrary) criteria described above is not constant for the six garnets: they are 3, 3, 3, 3, 5, 5 (Y modes), 4, 3, 3, 4, 3, 3 (X modes) and 3, 4, 4, 3, 2, 2 (neutral modes). These numbers, together with Figure 5, show that the simple correlation with the lattice parameter is lost; other variables (Si-O, X-O and Y-O distances, X and Y masses and ionic radii) superpose their influence on the frequencies and prevent from a simple correlation.

Some general trends can however still be identified. A linear boundary can be traced, dividing a low ν region containing modes mainly related to X motions, and a high ν region dominated by Y modes (see Figure 5). The dashed line representing this boundary starts at about 360 cm^{-1} for Prp and ends at about 220 cm^{-1} for Adr. The boundary frequency changes along the garnet family; the reason is mainly related to the masses of the X and Y cations: when passing from lighter Al (Prp, Alm, Sps, Grs) to heavier Cr (Uv) and Fe (Adr), the Y related frequencies undergo a downshift. In a similar way, Prp, with the lightest X cation (Mg), shows the highest X dominated frequencies (the exception is mode 10 of Adr, see below); Alm and Sps, containing the heaviest X cations (Fe and Mn respectively), exhibit coherently the lowest X dominated frequencies. Some exceptions can be found in the case of Uv and Adr, and correspond to modes featuring a coupled motion of different atomic types: mode 2 of both compounds has very low frequency (161.0 and 147.6 cm^{-1}, respectively) but is Y dominated; mode 10 of Adr is high frequency (366.7 cm^{-1}) but X dominated.

There is a final remark to be done concerning the behavior of the oscillator strengths in the low frequency region (below 200 cm^{-1}), dominated by the X cation motion. The Prp (modes 1 and 3), Alm (1 and 2) and Sps (1, 2 and 4) spectra show high intensity peaks in this region; this is not the case of Grs, Uv and Adr, whose X cation is Ca: its large ionic radius (1.12 Å) is probably responsible for a reduced motion within the X site, which in turn implies a reduced polarization of the corresponding normal modes.

CONCLUDING REMARKS

The vibrational properties and reflectance spectra of six members of the garnet family have been computed at the quantum mechanical ab initio level and compared with the corresponding extensive set of experimental data, involving 178 wavenumbers and 82 oscillator strengths.

It turns out that:

- The agreement among calculated and experimental wavenumbers ν_j is excellent; the mean

absolute difference $\overline{|\Delta|}$ ranges from 3.4 cm^{-1} (Grs) to 7.3 cm^{-1} (Adr) in the TO case, and from 3.4 cm^{-1} (Sps) to 6.8 cm^{-1} (Prp) in the LO case. The absolute difference $|\Delta\nu|$ between calculated and experimental values exceeds 15 cm^{-1} only in six cases, concerning either doubtful experimental assignments or low frequency modes.

- TO-LO splitting is confirmed to be an odd-defined issue. The one-to-one correspondence is meaningful for TO and LO peaks featuring high overlap (small W^{NA} contribution); in this case, computed and experimental assignments are in agreement, too. Whenever the overlap is smaller than 75% (high W^{NA} contribution), the one-to-one correspondence gains a high degree of arbitrariness.
- As regards the oscillator strengths f_j and their sum F, the comparison with experiments is delicate in the case of low frequency modes and of couples of modes very close in frequency; if these two issues are properly treated, the agreement improves significantly: the "amended" sum of absolute differences $\Delta F'$ ranges from 18% (Alm) to 27% (Grs) of the corresponding F'.
- High frequency modes are essentially SiO_4 tetrahedra internal motions; their wavenumbers are inversely related to the lattice parameter. Low frequency modes involve X and Y cations motions to a large extent. The number of X- and Y- dominated modes is not the same for the six garnets, and simple correlations cannot be established. X- and Y- dominated ranges of wavenumbers vary along the family, too; this trend relates with the different masses of the involved cations.
- Finally, ab initio simulation proves to be a powerful tool for the description of vibrational properties of large unit cell systems, such as aluminosilicates garnets. The overall quality of the simulation is well resumed by the impressive agreement among computed and experimental infrared reflectance curves.

ACKNOWLEDGMENTS

The authors are grateful to Prof. A.M. Hofmeister for providing the reflectance spectra and for helpful and fruitful discussions.

Figures

Figure 1 Reflectance spectra $R^{calc}(\nu)$ of Grs obtained with different sets of damping factors γ_j: all values set to $\overline{\gamma} = 9$ cm^{-1} (solid line), experimental values γ_j^{exp} taken from Hofmeister and Chopelas 1991a (dotted line), best-fit values γ_j^{fit} (dashed line). In all cases vibrational frequencies ν_j and oscillator strengths f_j are from our calculations. Experimental $R^{exp}(\nu)$ from McAloon and Hofmeister 1995 is also shown (thick grey solid line), for sake of comparison.

Figure 2 Calculated $R^{calc}(\nu)$ and experimental $R^{exp}(\nu)$ reflectance spectra. Computed curves are obtained by using a damping factor equal to 9 cm^{-1}. Experimental data are taken from Hofmeister et al. 1996 (Prp and Alm), Hofmeister and Chopelas 1991a (Sps) and McAloon and Hofmeister 1995 (Grs and Adr); experimental spectrum of Uv is not available.

Figure 3 Real and imaginary parts of the dielectric function $\varepsilon(\nu)$ of Adr; the imaginary part of $1/\varepsilon(\nu)$ is also shown. Note that the maxima of $\mathrm{Im}(\varepsilon(\nu))$ correspond to TO peaks whereas the minima of $\mathrm{Im}(1/\varepsilon(\nu))$ correspond to LO peaks.

Figure 4 Internal SiO_4 tetrahedra modes as a function of the lattice parameter. From left to right, here and in the following Figure, the six dots refer to Prp, Alm, Sps, Grs, Uv and Adr, respectively. Numbers to the left refer to the mode labels of Prp, given in Table 2. Modes 15-17: stretching. Modes 12-14: bending. Mode 11: twisting. Dots represent the frequencies of the six garnets; downwards bars Δ_{down} give the percent isotopic shifts (multiplied by 8, forsake of visibility) when the mass of the X cation is augmented by 20%; upwards bars Δ_{up} are the corresponding shifts when the mass of the Y cation is reduced by 20%. The absolute isotopic shifts are given in Table 11.

Figure 5 Effect of the isotopic shift on the ten lowest IR frequencies as a function of the lattice parameter. Chemical symbols above and below the top border indicate the X and Y cations of the six compounds, respectively. Dots represent the frequencies of the six garnets; downwards bars Δ_{down} give the percent isotopic shifts (multiplied by 2, for sake of visibility) when the mass of the X cation is augmented by 20%; upwards bars Δ_{up} are the corresponding shifts when the mass of the Y cation is reduced by 20%. Symbols are light grey when $\Delta_{up}/\Delta_{down} > 2$ and $\Delta_{up} > 3\%$ (Y dominated

modes), dark grey when $\Delta_{down}/\Delta_{up} > 2$ and $\Delta_{down} > 3\%$ (X dominated modes), black when none of these conditions is satisfied. The dashed line separates the light grey and dark grey regions. The absolute isotopic shifts are given in Table 12.

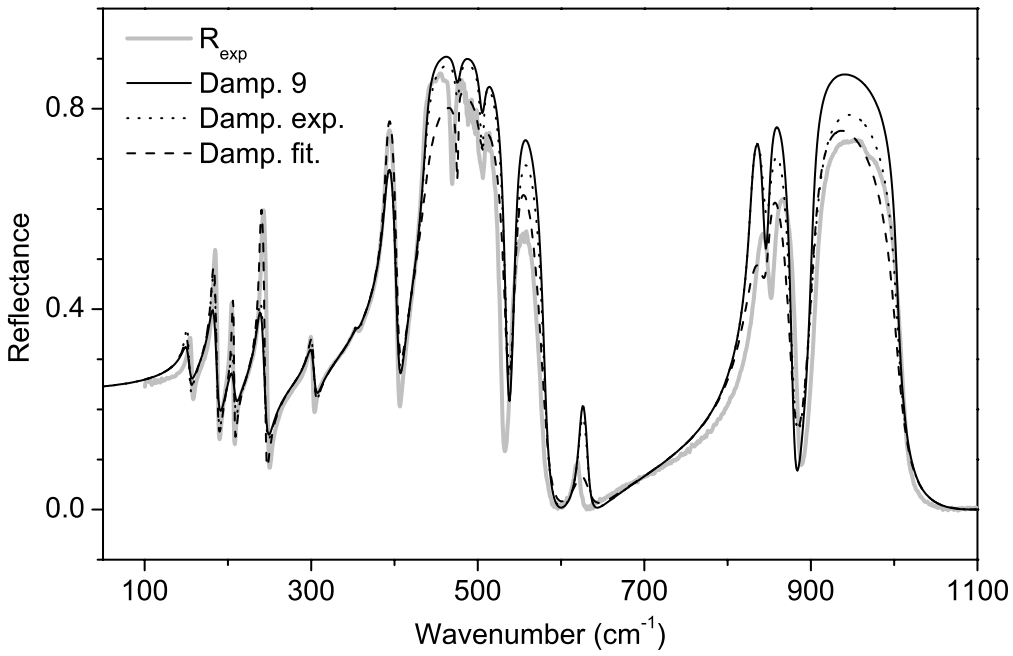

Figure 1

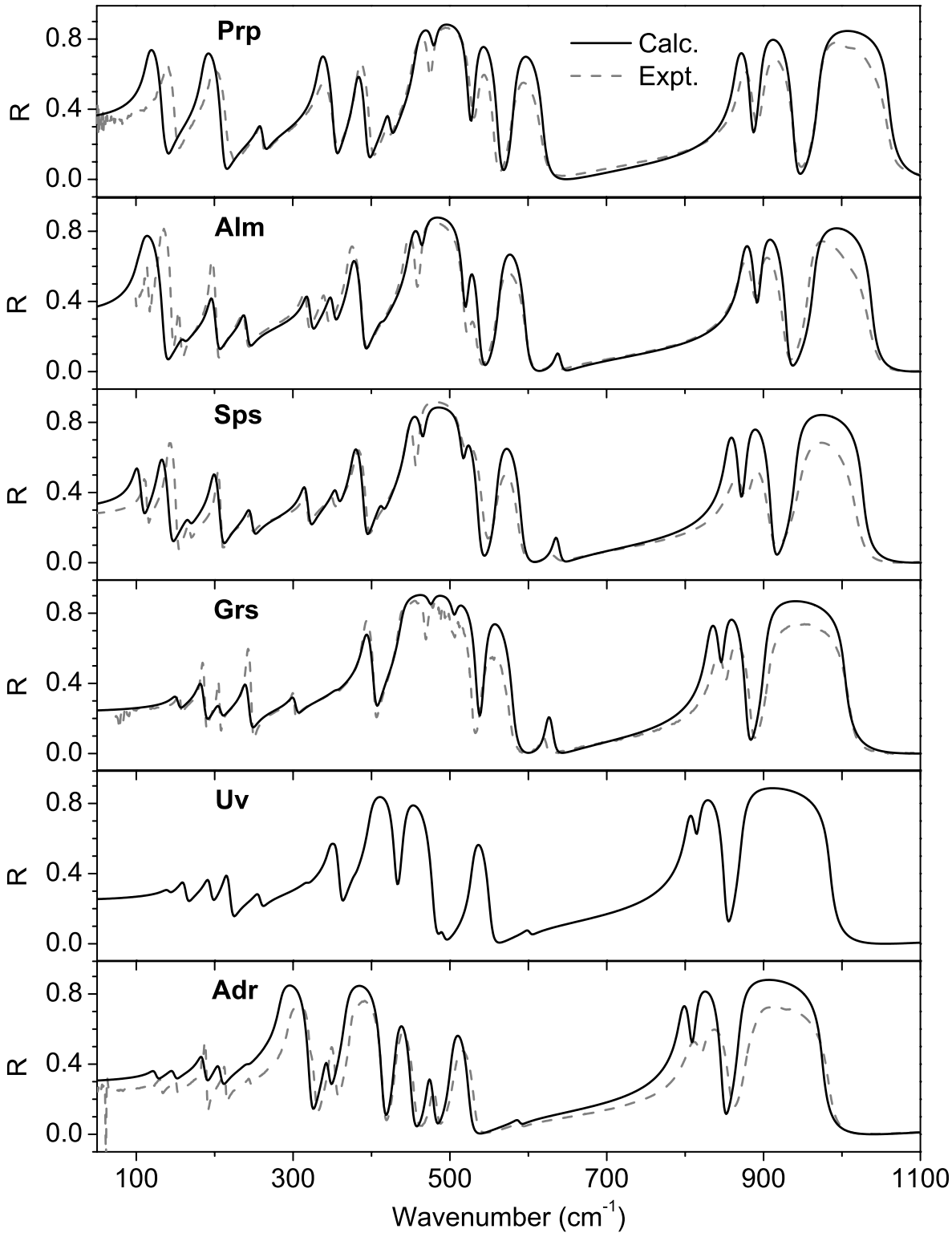
Prp
Calc.
Expt.
Alm
Sps
Grs
Uv
Adr
R
0.0
0.4
0.8
100
300
500
700
900
1100
Wavenumber (cm-1)

Figure 2

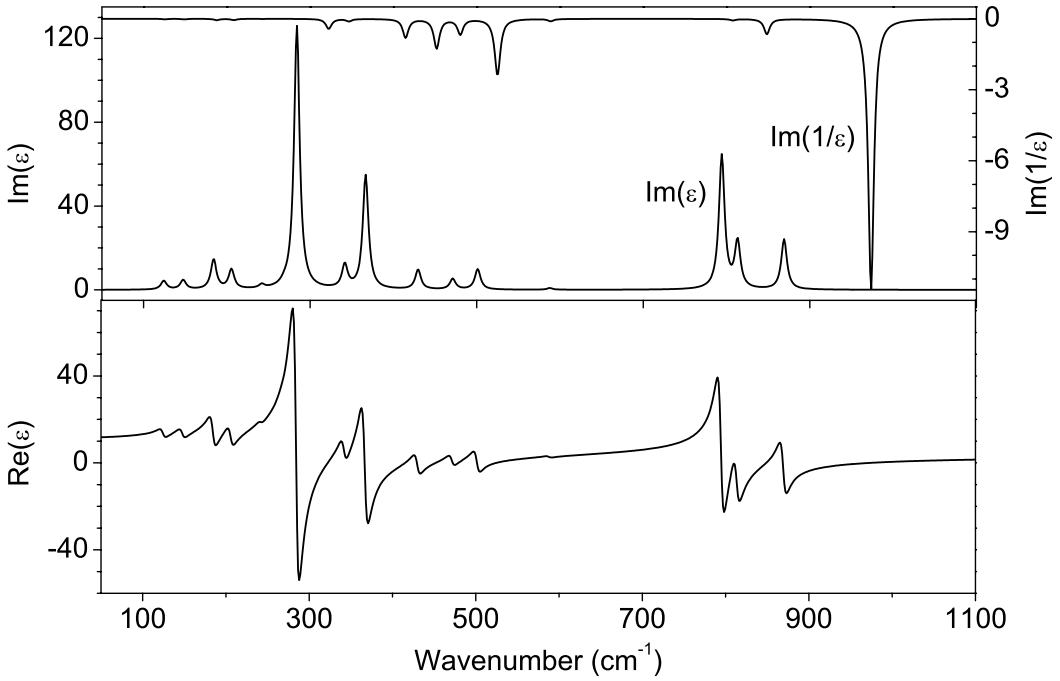
Im(ε)
Im(1/ε)
Re(ε)
Wavenumber (cm-1)
120
80
40
0
-3
-6
-9
-40
100
300
500
700
900
1100

Figure 3

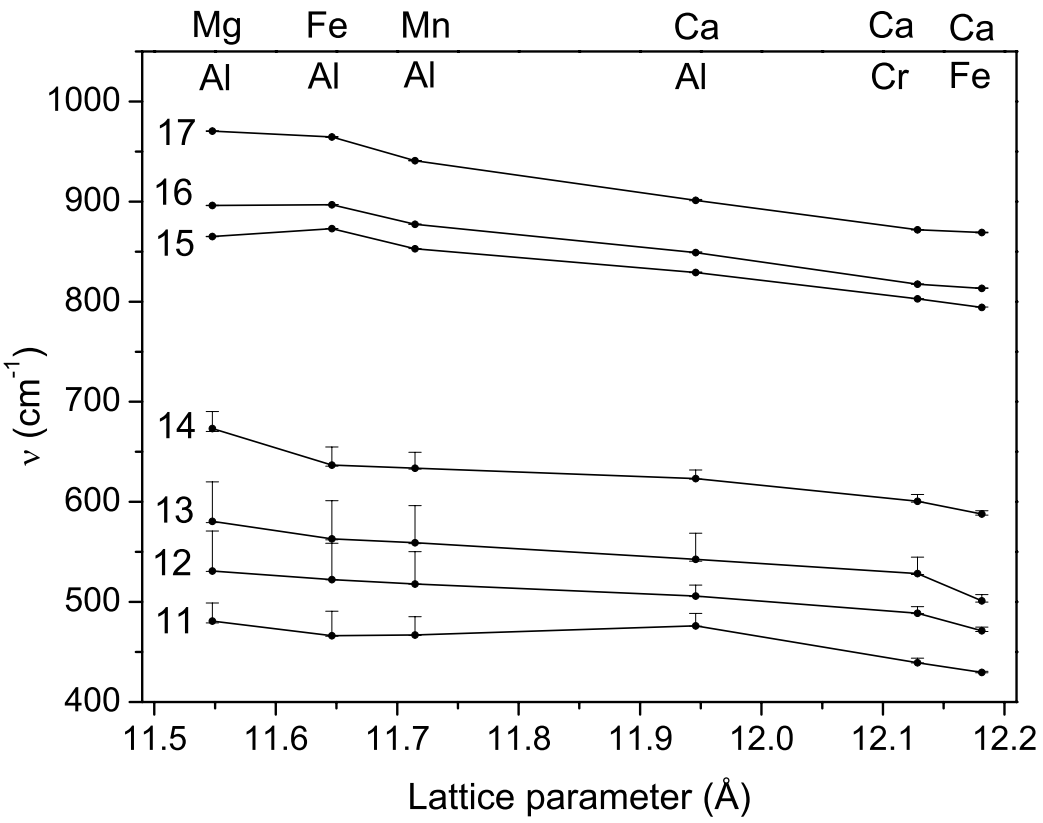
Mg Fe Mn Ca Ca Ca
Al Al Al Al Cr Fe
17
16
15
14
13
12
11
1000
900
800
700
600
500
400
ν (cm-1)
11.5 11.6 11.7 11.8 11.9 12.0 12.1 12.2
Lattice parameter (Å)

Figure 4

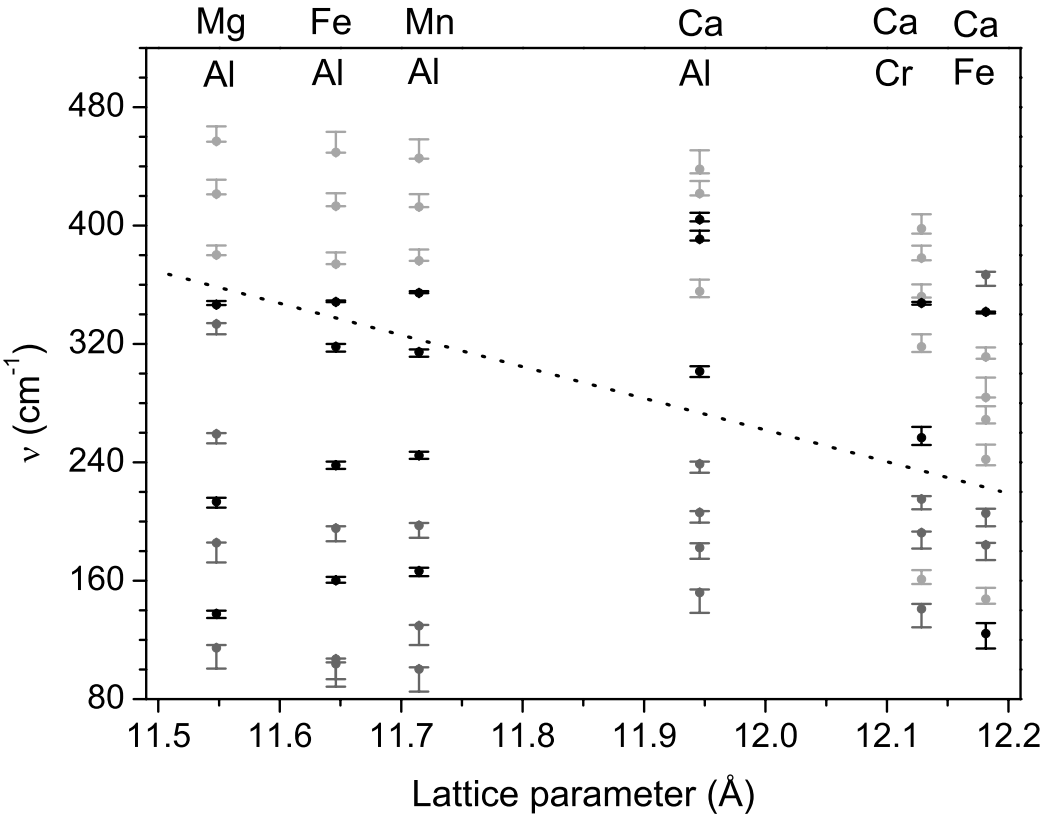
Mg
Fe
Mn
Ca
Ca
Ca
Al
Al
Al
Al
Cr
Fe
480
400
320
240
160
80
ν (cm-1)
11.5
11.6
11.7
11.8
11.9
12.0
12.1
12.2
Lattice parameter (Å)

Figure 5